ISSN 1063-7710, Acoustical Physics, 2019, Vol. 65, No. 3, pp. 322–333. © Pleiades Publishing, Ltd., 2019.

PHYSICAL FUNDAMENTALS OF ENGINEERING ACOUSTICS

Forming Low-Frequency Complete Vibration Bandgaps in a thin Nonmetallic Elastic Metamaterial Plate[1]

Suobin Li[a, *], Yihua Dou[a], Tianning Chen[b], Zhiguo Wan[a], Luyan Ju[a], Fan Zhang[c], and Xiao Xiao Cui[d]

[a] *School of Mechanical Engineering, Xi'an Shiyou University, Xi'an, Shaanxi, 710056 China*

[b] *School of Mechanical Engineering, Xi'an Jiaotong University, Xi'an, Shaanxi, 710049 China*

[c] *Xi'an Modern Chemistry Research Institute, Xi'an, Shaanxi, 710065, China*

[d] *Beijing Special Engineering Design and Research Institute, Beijing 100028, P. R. China*

**e-mail: ziyedeyan@stu.xjtu.edu.cn*

Received August 8, 2018; revised November 1, 2018; accepted December 26, 2018

Abstract—Low-frequency vibration-bandgaps in elastic metamaterials open new possibilities to minimize low-frequency vibration and noise. Unfortunately, fabricating a complete vibration bandgap for low frequencies still represents a challenging engineering task. In this paper, a new type of a low-frequency complete vibration bandgap in a thin non-metal elastic metamaterial plate is introduced and investigated numerically. The proposed elastic metamaterial plate consists of decoupling-resonators, which are deposited on a 2D, locally resonant phononic-crystal plate, made of an array of rubber fillers, which are embedded in a nonmetallic plate. The dispersion relationship, the power-transmission spectrum, and the displacement fields for the eigenmode are calculated using the finite element method. It is shown that coupling between the local resonance mode of the decoupling-resonators and the Lamb-wave mode of the epoxy plate, consistent with the modal superposition principle, is responsible for the formation of vibration bandgaps. Moreover, the equivalent spring-mass system for the coupling-resonators can be decoupled by introducing a rubber filler. In addition, both longitudinal and the transverse elastic wave bandgaps can be tuned to the same low-frequency range. As a result, a novel kind of low-frequency complete vibration bandgap, which can damp a low-frequency elastic wave, is produced. Furthermore, the effects of the decoupling-resonators on the vibration bandgap are investigated. It is now possible that an elastic metamaterial plate can be dampen with complete low-frequency vibration bandgaps, which can potentially be used for commercial noise and vibration reduction.

Keywords: elastic metamaterial plate, vibration bandgap, low-frequency vibration reduction, finite element method

DOI: 10.1134/S1063771019030084

1. INTRODUCTION

Phononic crystals (PCs) and locally resonant (LR) acoustic/elastic metamaterial (AMs/EMs) are types of functional structures that are designed to control acoustic/elastic waves in liquids/solids. They have attracted growing interest due to novel physical properties, such as acoustic/elastic wave bandgaps (BGs), where acoustic/elastic wave propagation is forbidden [1–3]. The existence of such BGs enables a variety of potential applications, in particular noise and vibration insulation [4–6]. It is known that there are two mechanisms that lead to the formation of BGs: Bragg scattering and the Localized resonance (LR). Because of Bragg scattering, PCs have a structuring period, which is of the same order as the wavelength of the forbidden frequencies. This means that large lattice constants are needed to reduce structural vibrations for low-frequencies. Unfortunately, this severely restricts the application of PCs in the audible frequency-range. To overcome this limitation, Liu et al. [13] proposed AMs/EMs, primarily based on the LR mechanism. The metamaterial consists of a heavy core with a soft epoxy matrix coating, and the associated wavelength is two orders of magnitude smaller than the Bragg bandgaps. A locally resonant bandgap (LRBGs) is related to the resonance frequency associated with scattering units, and it depends little on the periodicity and symmetry of the structure. Therefore, it is possible to bypass the limitation of Bragg bandgaps and generate bandgaps for low frequencies. Many studies of AMs/EMs have been reported [14–49].

The existence of low-frequency LRBGs enables elastic metamaterial to reduce low-frequency vibration and noise [14, 16]. In the past years, many elastic metamaterials were proposed that contain bandgaps in the low-frequency range [3–18]. Moreover, a large number of studies were done on low-frequency bandgaps in elastic metamaterial plate [19–39] because of

[1] The article is published in the original.

the many uses of plate structures in engineering. The elastic wave bandgap is also known as vibration bandgaps (including longitudinal and transverse wave bandgaps). Compared with the flat elastic metamaterial plate [19–22], the stubbed elastic metamaterial plate can shift the vibration bandgap to lower frequency range easily. Generally, the stubbed elastic metamaterial plate contains the one–side or double-sides elastic metamaterial plate. The one-sided elastic metamaterial plate consists of a square array of resonators on one side of a homogeneous plate and was first proposed by Wu et al. [23]. Later, many researchers investigated the effects of the resonators on the bandgap. Pennec et al. [24] and Oudich et al. [25] demonstrated that the mass effect of the resonators significantly affects the bandgap with respect to low frequencies. Zhang et al. [27] studied the geometric effects of the resonators on the bandgap with simple tapered resonators, and could produce lower BGs. Hsu et al. [28] studied bandgaps with simple neck-resonators and demonstrated that LRBGs and Bragg BG scan occur simultaneously. The double-sided elastic metamaterial plate consists of a square array of resonators on both sides of a homogeneous plate. It was first proposed by Assouar et al. [30]. The group demonstrated that it can increase the bandwidth and lower the bandgaps compared to the one-side elastic metamaterial plate.

Nevertheless, all the elastic metamaterial plates [23–37] discussed above were constructed by depositing one-sided or double-sided resonators on a homogeneous plate. Recently, Li et al. [38] proposed a one-sided elastic metamaterial plate made of a square-array of simple cylinder-resonators on one side of a 2D binary locally resonant PC plate. Compared with the classical one-sided elastic metamaterial plate, the bandgap studied in ref. [39] can be shifted to lower frequencies easily.

However, because there are three different modes for a plate, and they can only be coupled separately to special resonating modes of the resonators, such as the gaps for longitudinal elastic wave and transverse elastic wave plate modes can hardly be overlapped with each other in lower frequencies due to the coupling of the equivalent spring-mass system of the resonator, and thus the lower complete band gaps (including combined longitudinal and transverse wave bandgaps) are difficult to obtain [48]. As a result, the vibration bandgaps of these elastic metamaterial plates [23–48] are usually located in above 300 Hz. However, in practice, the frequency of most of the ambient vibration is distributed across a wide frequency-range (from 20 to 250 Hz) [39]. In order to obtain vibration bandgaps in this frequency range, Zhang et al. [40] proposed a novel elastic metamaterial plate with periodic spiral resonators. The group demonstrated that a transverse elastic wave bandgap can be moved to low frequencies (about 40 Hz), but a longitudinal elastic wave bandgap can only be located at higher frequencies. Furthermore, they cannot overlap to generate a complete vibration bandgap in the low-frequency range (below 100 Hz).

Thus, finding a way to adjust both the longitudinal and the transverse elastic wave bandgaps, such that they overlap at lower-frequencies, is an important stepping stone to control vibration. Only few studies were conducted on complete low-frequency vibration bandgaps below 100 Hz. In this paper, a novel kind of low-frequency complete bandgaps (including both the longitudinal and the transverse elastic wave bandgap) in an elastic metamaterial plate is introduced and investigated numerically. The proposed structure consists of decoupling-resonators, which are deposited on a 2D, locally resonant PCs plate, made of an array of rubber fillers embedded in an epoxy plate. The rubber filler and the decoupling-resonators are used to decouple the spring-mass system of the resonator and tune the longitudinal and the transverse elastic wave bandgaps. These can overlap to obtain complete vibration bandgaps in the low-frequency range. The dispersion relationship, the power-transmission spectrum and the displacement field of the eigenmodes were calculated using FEM. From this information we derive the formation mechanism and the composite taper resonator dependence of bandgaps.

This paper is organized as follows: In Section 2, we discuss the details of the model and the calculation method. Section 3 presents the numerical results and discussions. We then summarize the conclusions in Section 4.

2. MODEL AND CALCULATION METHOD

The proposed elastic metamaterial plate consists of a square array of decoupling-resonators on both sides of a 2D binary, locally resonant PC plate, which is made of an array of rubber fillers embedded in the epoxy plate. Figures 1a, 1b show a part of the proposed elastic metamaterial plate and its unit cell. In the proposed elastic metamaterial plate, the decoupling-resonators consist of the taper cap A and B, which is located on taper A. The geometrical parameters of the proposed elastic metamaterial plate are defined as follows. The diameter of the rubber filler, the epoxy-plate thickness and the lattice constant are denoted by D, e and a, respectively. The height and the diameter of the decoupling-resonators are denoted by h (h_A for taper A and h_B for taper B) and d (the upper diameter of composite taper resonators is denoted by d_{up}, and the lower diameter is denoted by d_{low}), respectively. The material parameters used in the calculations are listed in the Table. Both taper A and taper B consist of rubber and steel, respectively.

In order to investigate the bandgaps and resonant modes in the proposed elastic metamaterial plate, a series of the dispersion relationships were calculated using FEM, based on the Bloch theorem. This method has been used successfully in previous research [28, 29]. The commercial software, COMSOL Meta-

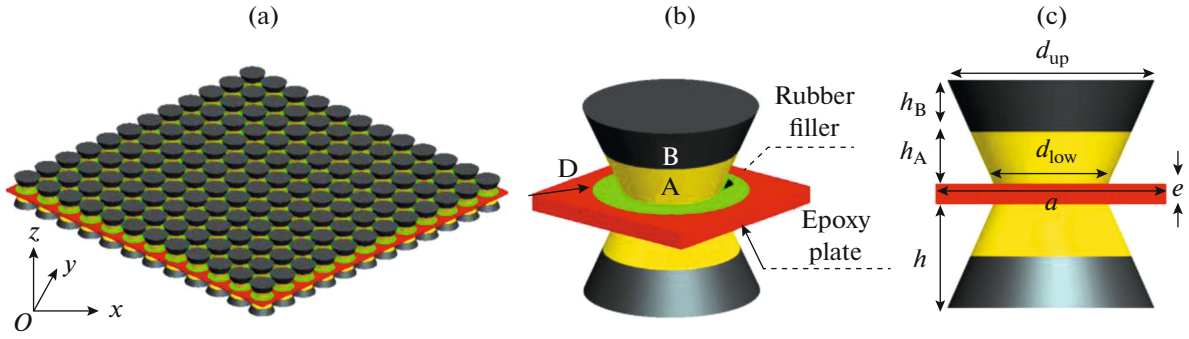

Fig. 1. Schematic of the proposed elastic metamaterial plate: (a) part of the structure, (b) unit cell, (c) front view of the unit cell.

physics version 3.5a was used to implement the FEM calculation instructions. The single unit cell, shown in Fig. 1b, is considered in the calculation on account of the periodicity of the structure. For the calculation of the band structure, the stress-free boundary conditions were applied to a free surface, and the periodic boundary conditions were applied to the boundaries between unit cells and their nearest cells, using the Bloch theorem

$$u_i(x+a, y+a) = e^{i(k_x a + k_y a)} u_i(x, y) \quad (i = x, y, z), \quad (1)$$

where the elastic displacement vector is denoted by u, the position vectors are denoted by x, y and z, while k_x and k_y are the Bloch wave vectors limited in the irreducible first Brillouin zone ($1BZ$). The Bloch calculation yields the eigenfrequencies and the corresponding eigenvectors, and the dispersion relationship can be obtained by changing the wave vector for the first irreducible Brillouin zone.

To further probe the existence of the longitudinal and transverse elastic wave BGs of the proposed structure, the transmission spectra for a structure with 6 units in x-direction was calculated using FEM. The acceleration excitation source is located at the left side of the finite structure and propagates excitations in the x-direction. The corresponding transmitted acceleration is recorded on the right side of the structure. The transmission spectrum is defined as

$$TL = 10\log\left(\frac{\alpha_0}{\alpha_i}\right), \quad (2)$$

where α_0 and α_i are the output and input accelerations of the plate, respectively. Finally, the transmission spectra can be obtained by changing the excitation frequency of the incident acceleration.

3. NUMERICAL RESULTS AND DISCUSSION

The band structures of the proposed elastic metamaterial plate is illustrated in Fig. 2a. The following structure parameters were used: $D = 8$, $e = 1$, $a = 10$, $h = 5$ ($h_A = h_B = 2.5$ mm), $d_{up} = 9$ and $d_{low} = 5$ mm.

We found fourteen bands within 0–400 Hz. Besides the traditional plate modes, which are longitudinal elastic wave modes (mainly the symmetric Lamb modes, such as S_2, S_4) and transverse elastic wave modes (mainly the anti-symmetric Lamb modes, such as A_2), many flat modes (such as S_1, S_3, A_1, f_1, f_2, f_3, f_4), which are the resonant modes of the composite taper resonator, were found. Five bandgaps (two longitudinal elastic wave bandgaps, one transverse elastic wave bandgap, two complete vibration bandgaps) form as a result of coupling the two modes above. The two longitudinal elastic wave bandgaps (the blue dashed areas mark the frequency bands without longitudinal elastic wave modes) are due to coupling between the longitudinal elastic wave modes (S_2, S_4) and the corresponding flat modes (S_1, S_3). The first one ranges from 53 to 103 Hz (between the 5th and 8th bands), while the second one ranges from 154 to 352 Hz (between the 9th and 14th bands). The absolute bandwidths for these are 50 and 198 Hz, respectively. The transverse elastic wave bandgap (the yellow dashed area marks the frequency bands without transverse elastic wave modes) is due to coupling between the transverse elastic wave modes (A_2) and the corresponding flat modes (A_2). It ranges from 59 to 318 Hz (between the 6th and 13th bands) with an absolute bandwidth of 259 Hz. The two complete vibration bandgaps (the red dashed areas mark the frequency ranges with neither longitudinal nor transverse elastic wave modes) are due to overlapping first and second longitudinal elastic wave bandgaps and the transverse elastic wave bandgap. The first one ranges from 59 to 103 Hz (between the 6th and 8th bands), while the second ranges from 154 to 318 Hz (between the 9th and 13th bands).

The flat modes, f_1, f_2, f_3, f_4, which corresponds to the flat bands, f_1, f_2, f_3, f_4, are extracted and displayed in Fig. 3. The corresponding vibrations of the flat bands shown in Fig. 3 are mainly the symmetry vibrations of the resonators. For example, mode f_1 represents a rotating vibration, which means that no reacting force acts on the plate. As a result, these flat

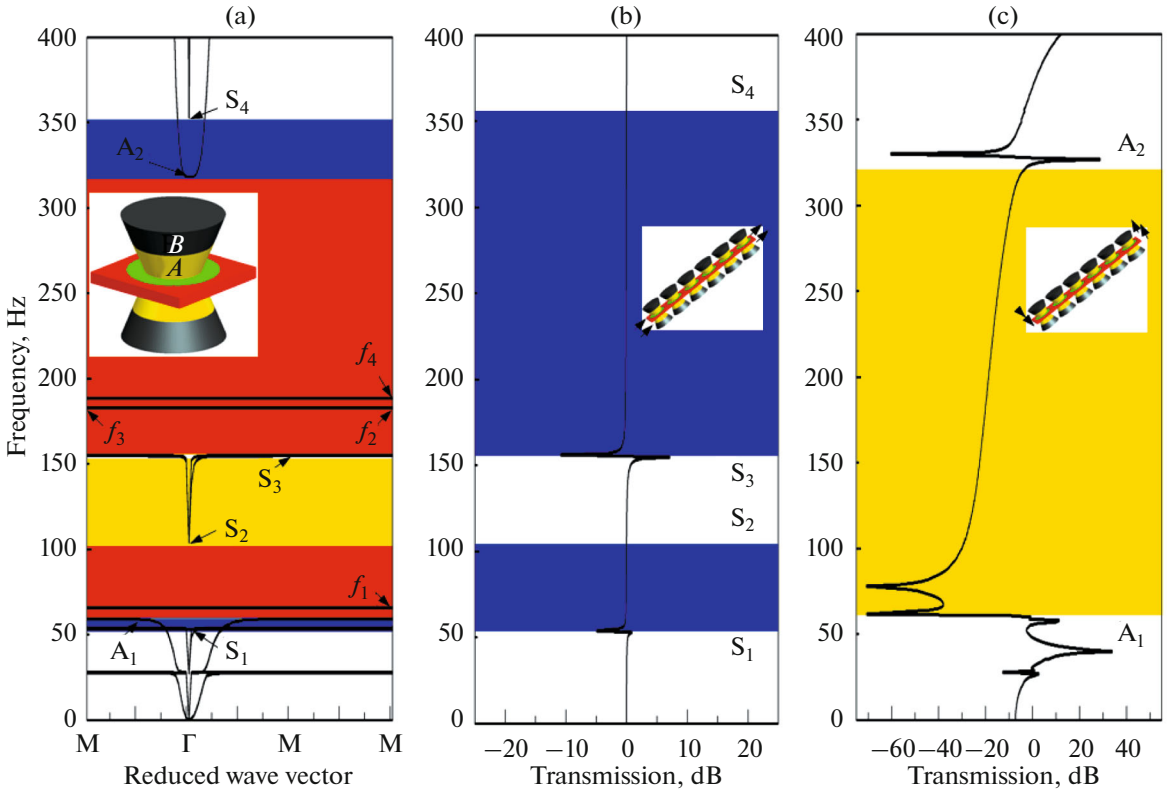

Fig. 2. Schematic of the band structures and the transmission-power spectra of the proposed elastic metamaterial plate: (a) band structures, (b) transmission-power spectra for longitudinal elastic wave vibration, (c) transmission-power spectra for transverse elastic wave vibration. The inset shows the schematic view of the unit cell of it. The red, blue, and yellow regions denote the complete, longitudinal and transverse elastic wave bandgaps, respectively.

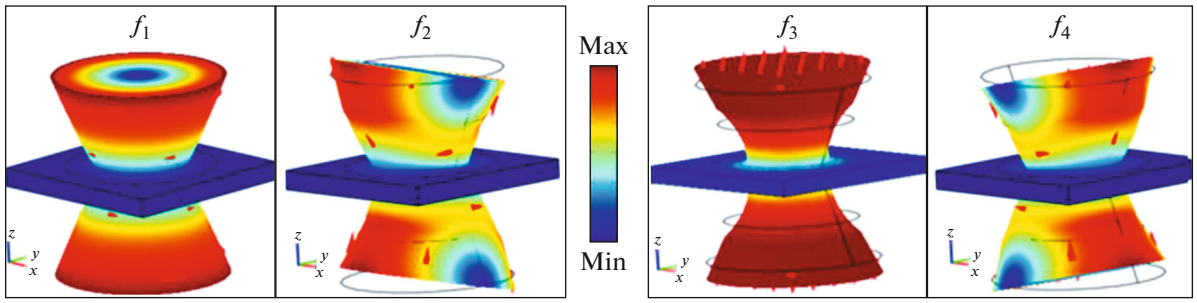

Fig. 3. The total displacement vector fields for the mode labeled in Fig. 2a: mode f_1; mode f_2; mode f_3; mode f_4.

modes do not affect the bandgaps. Although the flat modes can produce a bandgap due to the resonator, the bandwidth is zero because no reacting force acts on the plate. The frequency-ranges for the attenuation transmission spectrum of the longitudinal vibration is shown in Fig. 2b, and the transverse vibration, shown in Fig. 2c, demonstrate a perfect match with the longitudinal and the transverse elastic wave bandgaps. This also confirms the formation of the longitudinal and the transverse elastic wave bandgap of the proposed elastic metamaterial plate. However, the attenuation amplitude in the first complete vibration bandgap is larger than the second complete vibration bandgap, which effectively decreases vibration and noise. Hence, the following investigations focus only on the first complete vibration bandgap.

It can be observed that, compared with the "classical" elastic metamaterial plate, by introducing the composite taper resonators, the locations of both the longitudinal elastic wave and transverse elastic wave bandgaps are lowered. However, the transverse elastic wave bandgap always overlaps with the second longitudinal elastic wave bandgap. After introducing the rubber filler, the location of the longitudinal elastic

wave bandgap is kept stationary, but the transverse elastic wave bandgap is shifted to lower frequency (59 Hz) and overlaps with the first longitudinal elastic wave bandgap. Finally, a complete vibration bandgap is generated for low frequencies (below 100 Hz). Therefore, the composite taper resonators directly lowers the location of the longitudinal elastic wave-bandgaps (53 Hz), while the rubber filler directly lowers the location of the transverse elastic wave bandgaps (59 Hz). This causes the transverse elastic wave bandgaps to overlap with the first longitudinal elastic wave bandgap, which produces a complete vibration bandgap for lower frequencies.

A. Forming Mechanisms of the Low-Frequency Vibration Bandgaps

To study the physical mechanism for the occurrence of the complete low-frequency vibration bandgap in the proposed elastic metamaterial plate, several specific resonance modes (A_1, S_1), which correspond to the lower edge of the first vibration bandgap (longitudinal and transverse elastic wave bandgaps), and several specific traditional plate modes (A_2, S_2), which correspond to the upper edge of the first vibration bandgap (longitudinal and transverse elastic wave bandgap), are extracted.

Figure 6 shows the magnitude of the total displacement vector of a unit cell of the proposed elastic metamaterial plate (Fig. 6a), the transition elastic metamaterial plate (Fig. 6b), and the classical elastic metamaterial plate (Fig. 6c), respectively. They correspond to the upper and lower edges of the transverse elastic wave bandgap for each structure. The mode A_2 is an anti-symmetric Lamb mode of the epoxy plate. The epoxy plate vibrates along the z-axis, while the resonator remains stationary. For these frequencies, the anti-symmetric Lamb mode is activated, and the transverse elastic wave propagates through the elastic metamaterial plate as a anti-symmetric Lamb mode. When the frequency of the transverse elastic wave approaches the first natural frequency of the composite taper resonator, the resonant mode A_1 becomes active. The composite taper resonator vibrates along the z direction and generates a reaction force on the plate and prevent the plate vibrates in z direction. In this case, the transverse elastic wave cannot propagate through the elastic metamaterial plate. As a result, a transverse elastic wave bandgap appears. Within the transverse elastic wave bandgap, the reaction force still acts on the plate and prevents the transverse elastic wave from propagating. When the frequency of the transverse elastic wave deviates from the natural frequency of mode A_1, using the modal superposition principle [41] we can formulate:

$$z = \eta_{A_{11}}A_1 + \eta_{A_{22}}A_2 + \ldots + \eta_{A_{nn}}A_n, \qquad (3)$$

where z denotes the response of the plate and η_{Ann} denotes the modal participation factor for mode A_n. The modal participation factors η_{A11} for mode A_1 decrease and weaken the reaction force until it disappears. Then, the anti-symmetric Lamb mode A_2 is released again. As a result, the transverse elastic wave bandgap closes.

Details of the transverse elastic wave propagation that form the transverse elastic wave bandgap are shown in Fig. 7. The frequency range (0–600 Hz) is divided into five intervals (ω_1, ω_2, ω_3, ω_4, ω_5). The excitation frequency starts at 0 Hz and gradually reaches 600 Hz:

(1) Interval ω_1. When the excitation frequency increases, the modal participation factor η_{A-1-1} of the anti-symmetric Lamb mode A_{-1} increases. This causes the anti-symmetric Lamb mode A_{-1} to be amplified and converted into the main mode of the system. For certain frequencies (interval ω_1), the anti-symmetric Lamb mode A_{-1} becomes active and the transverse elastic wave propagates through the elastic metamaterial plate in the anti–symmetric Lamb mode A_{-1}. This way, no transverse elastic wave bandgap is produced.

(2) Interval ω_2. When the excitation frequency increases, the modal participation factor η_{A-1-1} of the anti–symmetric Lamb mode A_{-1} decreases but the modal participation factor η_{A+1+1} of the anti-symmetric Lamb mode A_{+1} increases. This causes the anti-symmetric Lamb mode A_{+1} to be amplified and converted into the main mode of the system. For certain frequencies (interval ω_2), the anti-symmetric Lamb mode A_{+1} becomes active and the transverse elastic wave propagates through the elastic metamaterial plate in the anti-symmetric Lamb mode A_{+1}. This way, no transverse elastic wave bandgap is produced.

(3) Interval ω_3. When the excitation frequency increases, the modal participation factor η_{A-1-1} and η_{A+1+1} decrease, but the modal participation factor η_{A11} of the resonant mode A_1 increases. This causes the resonant mode A_1 to be amplified and converted into the main mode of the system. Towards the end of the frequency range (intervals ω_3), the composite taper resonator vibrates along the z direction and generates a reacting force to the plate, and against the plate vibrates along the z direction. In this case, the transverse elastic wave cannot propagate through the elastic metamaterial plate. As a result, a transverse elastic wave bandgap opens up.

(4) Interval ω_4. When the excitation frequency increases, the modal participation factor $\eta_{A-1-1,}$ η_{A+1+1} and η_{A11} decrease but the modal participation factor η_{A11} of the resonant mode A_1 is larger than the modal participation factor η_{A-1-1} and η_{A+1+1}. This causes the resonant mode A_1 to continue to act as a main mode of the system. For certain frequencies

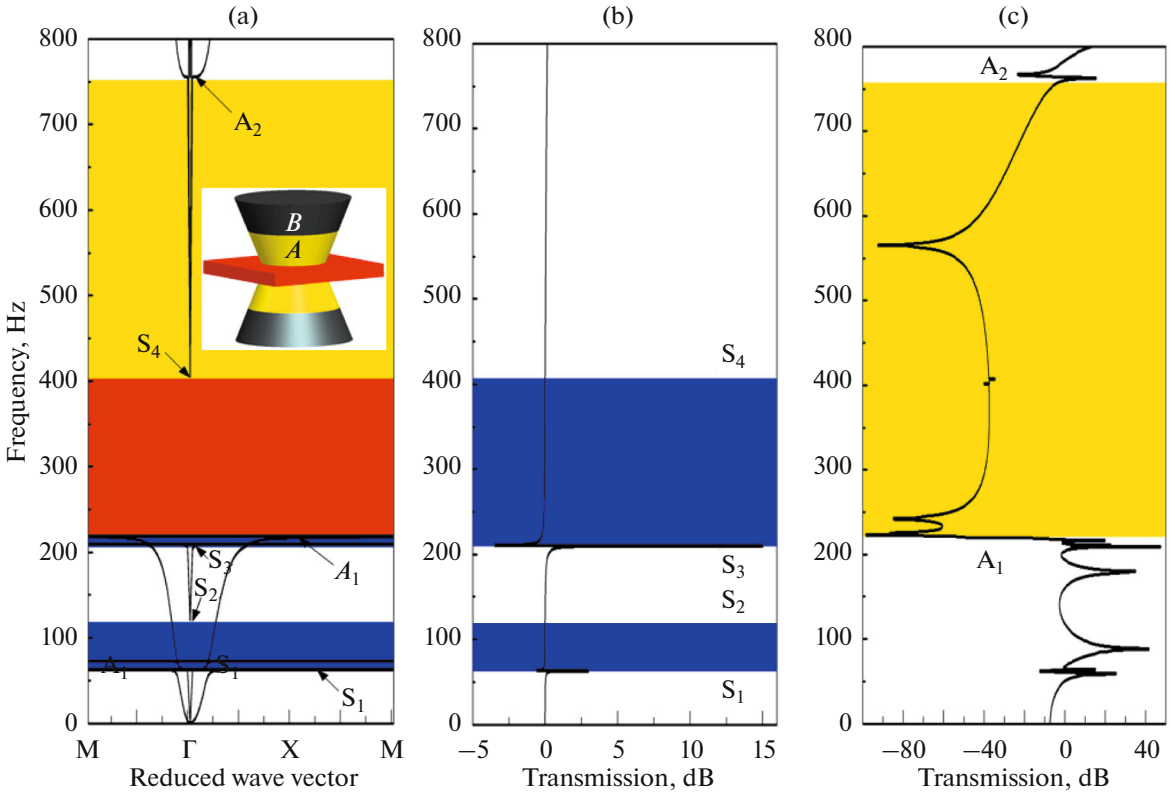

Fig. 4. Schematic of the band structures and the transmission-power spectra of the "transition" elastic metamaterial plate: (a) band structures, (b) transmission-power spectra for longitudinal elastic wave vibration, (c) transmission-power spectra for transverse elastic wave vibration. The insets show a schematic of the unit cell. The red, blue and yellow regions denote the complete, longitudinal and transverse elastic wave bandgaps, respectively.

(interval ω_4), the reacting force still acts on the plate and prevents the propagation of the transverse elastic wave. When the frequency of the transverse elastic wave deviates from the natural frequency of mode A_1, the modal participation factors η_{A1l} for the mode A_1 becomes small and weakens the reaction force until it disappears. Then, the anti-symmetric Lamb mode A_2 is released again. As a result, the transverse elastic wave bandgap closes. This formation mechanism for the transverse elastic wave bandgaps is shown in Fig. 8. As the frequency of the transverse elastic wave deviates from the natural frequency of the resonator mode, its modal participation factors decreases (the modal participation factor η_{A1l} of the resonant mode A_1 changes from one to zero) and generates a reaction force that decreases until it disappears. Then, the transverse elastic wave bandgap closes.

In other words, the transverse elastic wave bandgap of the system appears because of the coupling between the flat mode A_1 and the anti-symmetric Lamb mode A_2. This process follows the modal superposition principle.

The opening location of the transverse elastic wave bandgap is determined by the natural frequency of the resonant mode A_1. The vibration process of the resonant mode A_1 can be regarded as a mass-spring system—see Fig. 6. For the classical and the transition elastic metamaterial plates, the rubber taper acts as a spring, while the steel taper acts as a mass. Because the rubber taper is less stiff than the cylinder rubber, the opening location of the transverse elastic wave bandgap shifts to lower frequencies. For the proposed elastic metamaterial plate, the displacement fields are distributed among all composite taper resonators and produces an analogous-rigid mode for all composite taper resonators. This occurs because the whole composite taper resonator bulk moves along the z-axis. As a result, the rubber filler acts as a spring and the whole composite taper resonator bulk acts as a mass. Thus, the frequencies decrease.

Figure 9 shows the magnitude of the total displacement vectors for a unit cell of the proposed elastic metamaterial plate (Fig. 9a), the transition elastic metamaterial plate (Fig. 9b) and the classical elastic metamaterial plate (Fig. 9c), respectively. These correspond to the upper and lower edges of the first longitudinal elastic wave bandgap for each elastic metamaterial plate. The mode S_2 represents a symmetric Lamb mode of the plate. The epoxy plate vibrates along the xy-plane, while the resonators swing in the opposite direction. For certain frequencies, the symmetric Lamb mode S_2 becomes active and the longitu-

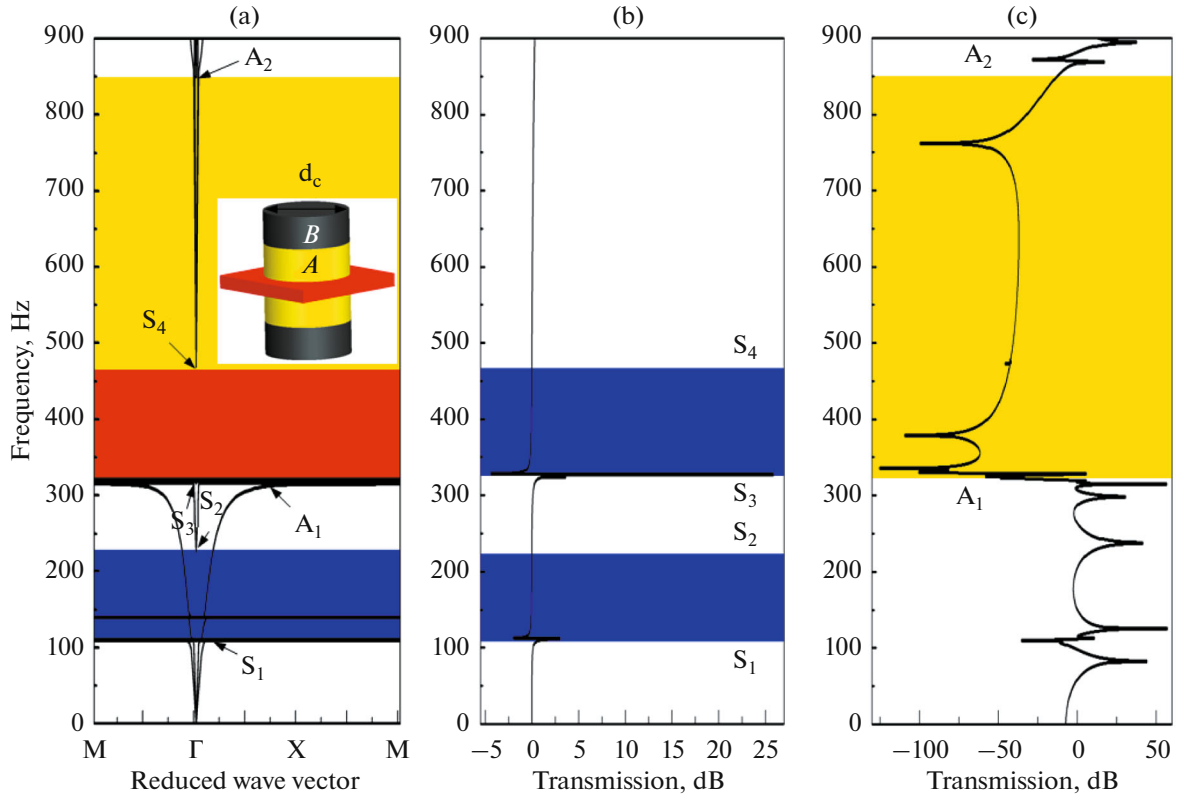

Fig. 5. Schematic of the band structures and the transmission-power spectra of the "classical" elastic metamaterial plate: (a) band structures, (b) transmission-power spectra for longitudinal elastic wave vibration, (c) transmission-power spectra for transverse elastic wave vibration. The insets show a schematic of the unit cell. The red, blue, and yellow regions denote the complete, longitudinal and transverse elastic wave bandgaps, respectively. $d_c = 7$ mm.

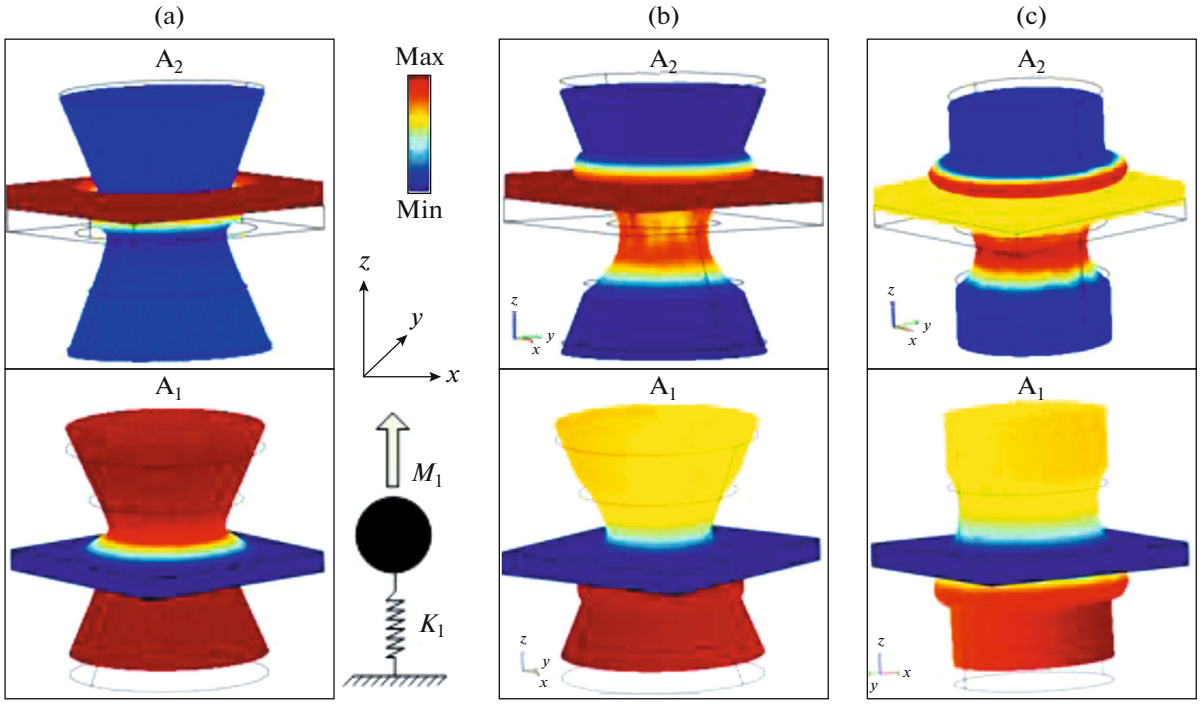

Fig. 6. The total displacement vector fields of the modes (resonant mode A_1 and anti-symmetric Lamb mode A_2): (a) corresponds to Fig. 2a, (b) corresponds to Fig. 4a, and (c) corresponds to Fig. 5a.

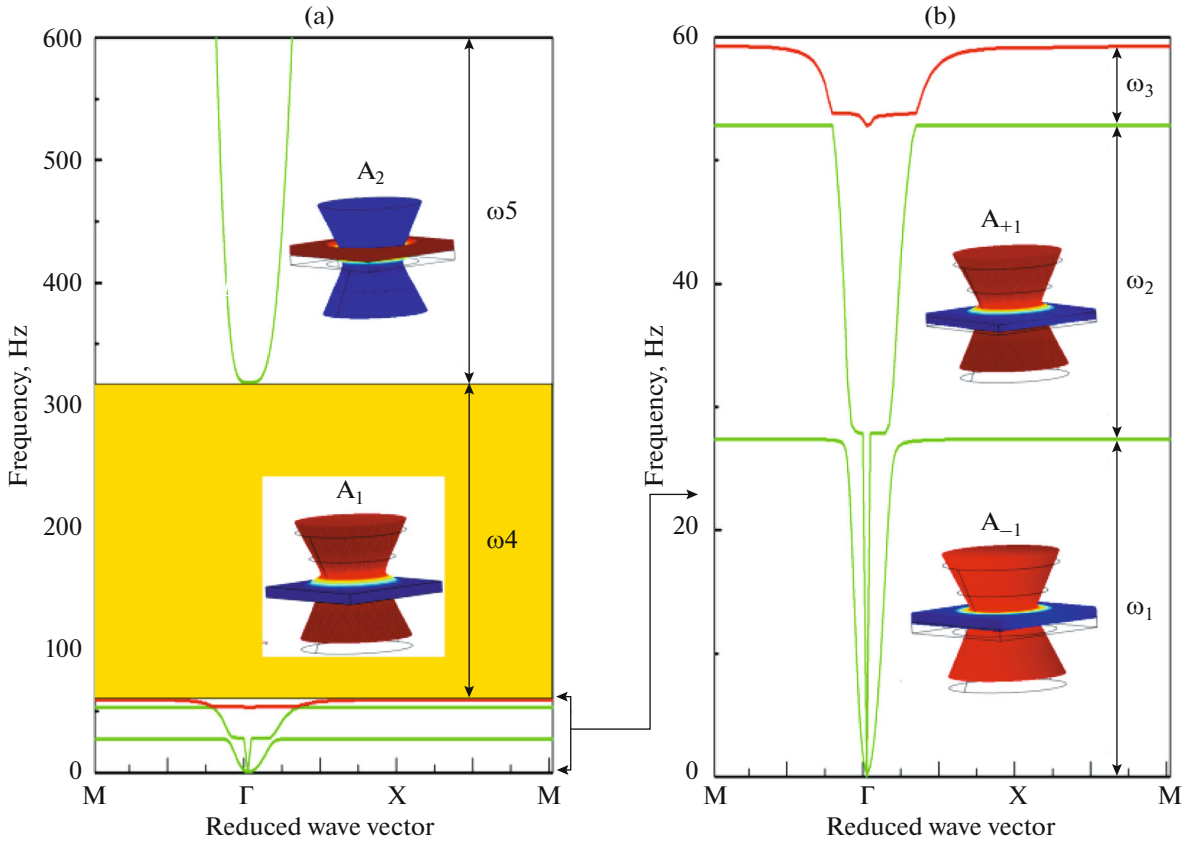

Fig. 7. Propagation of the transverse elastic wave during the formation of a transverse elastic wave bandgap.

dinal elastic wave propagates through the elastic metamaterial plate as a symmetric Lamb mode. When the frequency of the longitudinal elastic wave approaches the first natural frequency of the resonator, the resonant mode S_1 becomes active. The resonators swing along a plane, which is vertical to the *xy*-plane. This produces a reaction force on the plate to prevent the plate from vibrating along *xy*-plane. In this case, the longitudinal elastic wave cannot propagate through the elastic metamaterial plate. As a result, a longitudinal elastic wave bandgap appears. Within the longitudinal elastic wave, the reaction force still acts on the plate and prevents the longitudinal elastic wave from propagating. When the frequency of the longitudinal elastic wave deviates from the natural frequency of the resonant mode S_1, using the modal superposition principle [41], we can formulate:

$$xy = \eta_{S_{11}} S_1 + \eta_{S_{22}} S_2 + \ldots + \eta_{S_{nn}} S_n, \quad (4)$$

where *xy* denotes the response of the plate and η_{Snn} denotes the modal participation factor of the mode S_n. The modal participation factor η_{S11} of the mode S_1 becomes small and weakens the reaction force until it disappears. Subsequently, a symmetric Lamb mode S_2 is released again and, as a result, the longitudinal elastic wave bandgap closes.

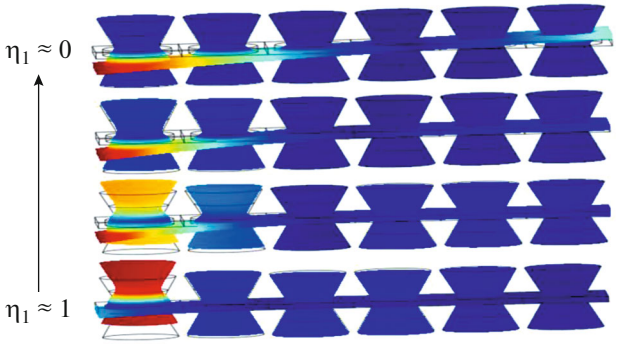

Fig. 8. Formation mechanism for the transverse elastic wave bandgaps.

Details of the longitudinal elastic wave propagation for the formation of a longitudinal elastic wave bandgap are shown in Fig. 10. The frequency range (0–600 Hz) is divided into six intervals (ω_1, ω_2, ω_3, ω_4, ω_5, ω_6). The excitation frequency starts at 0 Hz and gradually reaches 600 Hz:

(1) Interval ω_1. When the excitation frequency increases, the modal participation factor η_{S-1-1} of the symmetric Lamb mode S_{-1} increases. This causes the symmetric Lamb mode S_{-1} to be amplified and con-

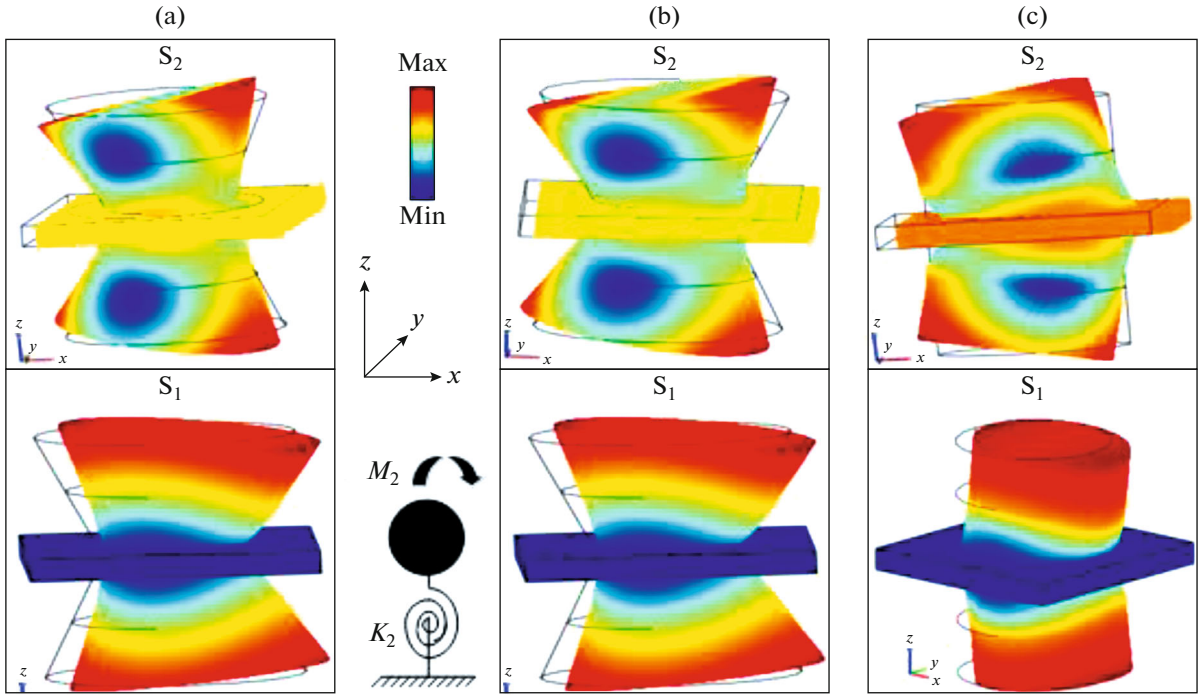

Fig. 9. Total displacement vector fields of the modes (resonant mode S_1, symmetric Lamb mode S_2): (a) corresponds to Fig. 2a, (b) corresponds to Fig. 4a, and (c) corresponds to Fig. 5a.

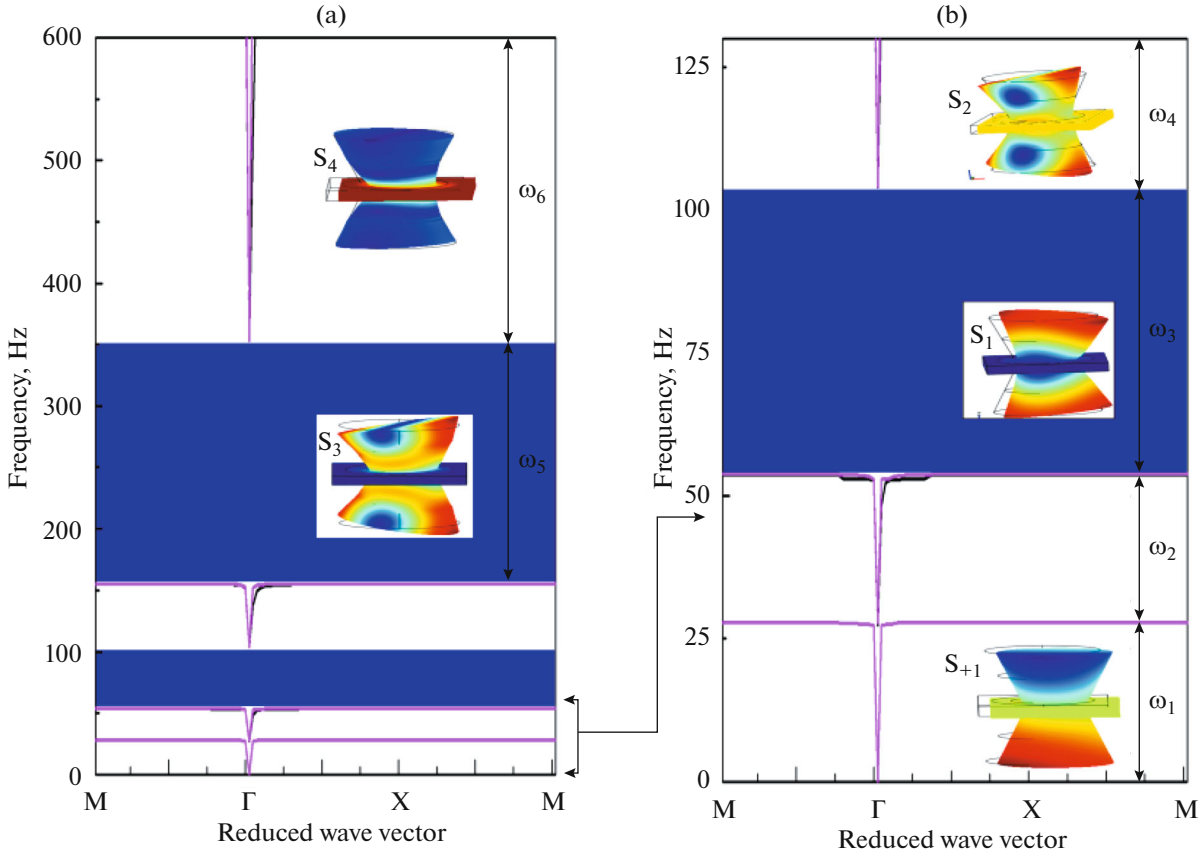

Fig. 10. Propagation process for the longitudinal elastic wave with respect to the formation of a longitudinal elastic wave bandgap.

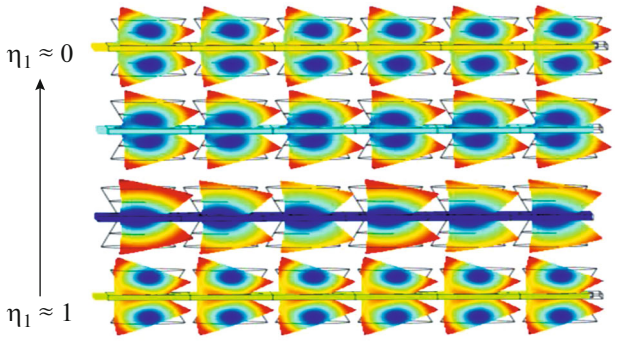

Fig. 11. Formation mechanism of the longitudinal elastic wave bandgaps.

verted into the main mode of the system. For certain frequencies (interval ω_1), the symmetric Lamb mode S_{-1} is active and the longitudinal elastic wave propagates through the elastic metamaterial plate as a symmetric Lamb mode S_{-1}. As a result, no longitudinal elastic wave bandgap appears.

(2) Interval ω_2. When the excitation frequency increases, the modal participation factor η_{S+1+1} decreases but the modal participation factor η_{S11} of the resonant mode S_1 increases. This causes the resonant mode S_1 to be amplified and converted into the main mode of the system. Towards the end of the frequency range (interval ω_2), the composite resonator swings along a plane, which is vertical to the *xy*-plane. This produces a reaction force on the plate that prevents the plate from vibration along the *xy*-plane. In that case, the longitudinal elastic wave cannot propagate through the elastic metamaterial plate. As a result, a longitudinal elastic wave bandgap appears.

(3) Interval ω_3. When the excitation frequency increases, the modal participation factors η_{S+1+1} and η_{S11} decrease but the modal participation factor η_{S11} of the resonant mode S_1 becomes larger than the modal participation factor η_{S+1+1}. This causes the resonant mode S_1 to continue to act as a main mode of the system. For certain frequencies (interval ω_3), the reaction force still acts on the plate and hinders the propagation of the longitudinal elastic wave. When the frequency of the longitudinal elastic wave deviates from the natural frequency of the mode S_1, the modal participation factor η_{S11} for mode S_1 decreases and weakens the reaction force until it disappears. Subsequently, the symmetric Lamb mode S_2 is released again. As a result, the longitudinal elastic wave bandgap closes. This formation mechanism for the longitudinal elastic wave bandgaps is shown in Fig. 11. As the frequency of the longitudinal elastic wave deviates from the natural frequency of the resonator mode, the modal participation factors become smaller (the modal participation factor η_{S11} of the resonant mode S_1 decrease from one to zero) and causes the reaction force to decrease and disappear. Hence, the longitudinal elastic wave bandgap closes. It expressed as the end of a finite periodic structure changes from rest to motion.

As a result, we conclude that the longitudinal elastic wave bandgap of the system is formed due to coupling between the flat mode S_1 and the symmetric Lamb mode S_2—based on the modal superposition principle.

The opening location of the longitudinal elastic wave bandgap is determined by the natural frequency of the resonant mode S_1. The vibration process for the resonant mode S_1 can be understood as a mass-spring system (see Fig. 9). For the proposed elastic metamaterial plate, the rubber taper acts as a spring, and the steel taper acts as a mass. Because the rubber taper is less stiff than the rubber cylinder, the opening location of the longitudinal elastic wave bandgap decreases.

Two low frequency vibration bandgaps (the longitudinal elastic wave bandgap and the transverse elastic wave bandgap) overlap to form a low-frequency complete vibration bandgap, where both the longitudinal and the transverse elastic wave are not allowed.

B. Effect of the Decoupling-Resonators on the Vibration Bandgaps

To obtain a lower and a larger frequency bandgaps, we investigate the effect of the decoupling-resonators on the vibration bandgaps of the proposed elastic metamaterial plate in more detail. In particular, the effect of steel taper height on the vibration bandgaps is examined.

First, we investigate the effect of steel tappr height on the first transverse elastic wave bandgap. Figure 12 shows the evolution of the first transverse elastic wave bandgap as a function of the steel taper height h_S. We can find that, with increasing steel taper height, the lower edge of the first transverse elastic wave bandgap shifts to lower frequencies, while the upper-edge shifts to lower frequencies first but then to higher frequen-

Table 1. Material parameters used for the calculations

Material	Mass density, kg/m^3	Young's modulus, 10^6 N/m^2	Poisson's ratio
Epoxy	1180	4350	0.3679
Steel	7800	210000	0.29
Rubber	1300	0.1175	0.47

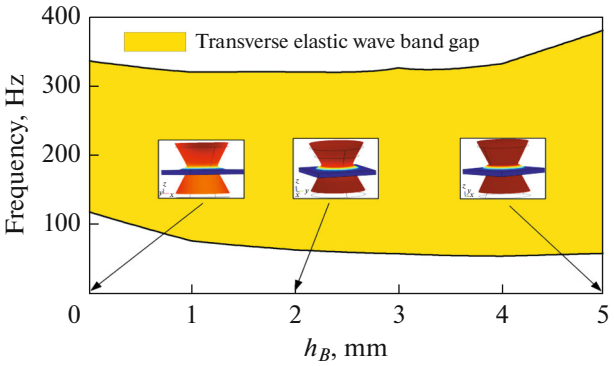

Fig. 12. Evolution of the first transverse elastic wave bandgap in the proposed elastic metamaterial plate as a function of steel taper height.

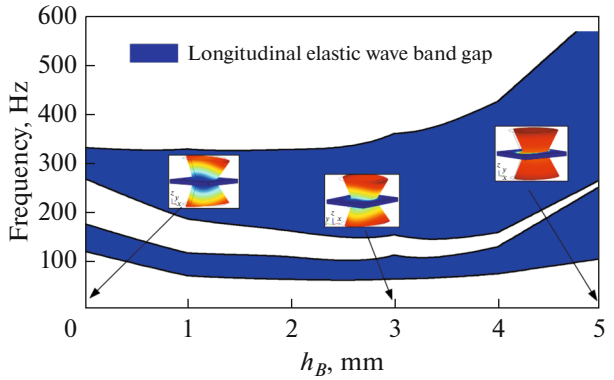

Fig. 13. Evolution of the first and second longitudinal elastic wave bandgap in the proposed elastic metamaterial plate, as a function of the steel taper height.

cies. This causes the bandwidth to become wider, and the gap location shifts to lower frequencies.

The above effect can be explained using the displacement fields of the flat mode A_1, which corresponds to the lower edge of the transverse elastic wave bandgap with different steel taper heights. It can be seen in Fig. 12 that, when the steel taper height increases, the resonant vibration of the composite resonator behaves like an "analogous-rigid mode" of the whole decoupling-resonators because its bulk moves along the z-axis direction. As the height of the steel taper increases, the lumped mass increases, while the spring stiffness keeps constant. Furthermore, the lower edge of the transverse elastic wave bandgap shifts to lower frequencies, and the coupling between the flat mode A_1 and the anti-symmetric Lamb mode A_2 increases. Ultimately, the bandwidths of the transverse elastic wave become wider.

Next, we studied the effect of the steel taper height on the first and second longitudinal elastic wave bandgaps. Figure 13 shows the evolution of the first and the second longitudinal elastic wave bandgaps as a function of the steel taper height h_S. Clearly, as the steel taper height increases, both the lower and the upper edges of the first and second longitudinal elastic wave bandgaps shift to lower frequencies before they move to higher frequencies. For example, when the steel taper height is less than or equal to 3 mm, the lower edges shift to lower frequencies with increasing steel taper height. However, when the steel taper height is larger than 3 mm, their lower and upper edges shift to higher frequencies.

These phenomena can be explained using the displacement fields of the flat mode S_1, which corresponds to the lower edge of the first longitudinal elastic wave bandgap with different steel taper heights. It can be seen in Fig. 13 that, when the steel taper height increases, the resonant mode of the decoupling-resonators vibrates as bending vibration before it vibrates as an analogous-rigid mode of the resonator, along the xy-plane. For the first mode, the rubber taper stub acts as a spring, while for the latter, the rubber filler acts as a spring. Compared to these, the rubber filler in the xy-plane is stiffer than the rubber stub, and the coupling between the flat mode S_1 and the Lamb mode S_2 increases. This causes the longitudinal elastic wave bandgap to shift to higher frequencies and increase the bandwidth.

4. CONCLUSIONS

In this paper, a novel kind of a low-frequency complete vibration bandgap in an elastic metamaterial plate, which consists of a decoupling-resonators deposited on a 2D locally resonant PCs plate, was introduced and studied numerically. The following conclusions can be drawn.

The coupling between the local resonance mode of the decoupling-resonators and the Lamb wave modes (longitudinal and transverse elastic wave modes), which obeys the modal superposition principle, is responsible for the formation of the vibration bandgaps (longitudinal and transverse elastic wave bandgaps).

The equivalent spring-mass system of the coupling-resonators can be decoupled by introducing a rubber filler, and the longitudinal and the transverse elastic wave bandgaps can be shifted to the same low-frequency range.

The transverse and the longitudinal elastic wave bandgaps can overlap. As a result, a low-frequency complete vibration bandgap, which ranges from 59 to 103 Hz, is obtained.

The effect of the decoupling-resonators on the vibration bandgaps is investigated. Our results show that the location of the complete vibration bandgaps can be shifted to a significantly lower frequency-range, and the bandwidth can be expanded into a much larger frequency range by introducing different decoupling-resonators.

The proposed elastic metamaterial plate provides an effective way, for elastic metamaterial plates, to produce complete vibration bandgaps for low frequencies. These results open new possibilities for commercial vibration and noise reduction.

ACKNOWLEDGMENTS

The authors gratefully acknowledge financial support from the Project of National Natural Science Foundation of China (no. 51275377). We would like to thank Dr. Linkai Niu for his kind comments to improve the paper.

REFERENCES

1. M. Sigalas and E. N. Economou, Solid State Commun. **86**, 141 (1993).
2. Y. Tanaka and S. I. Tamura, Phys. Rev. B **58**, 7958 (1998).
3. J. H. Ma, Z. L. Hou, and B. M. Assouar, J. Appl. Phys. **115**, 093508 (2014).
4. A. Khelif, B. Djafari-Rouhani, V. Laude, and M. Solal, J. Appl. Phys. **94**, 7944(2003).
5. L. Cremer, M. Heckl, B. A. T. Petersson, and P. J. Remington, J. Acoust. Soc. Am. **118**, 2754 (2005).
6. J. H. Ma, Z. L. Hou, and B. M. Assouar, J. Appl. Phys. **115**, 093508(2014).
7. M. S. Kushwaha, P. Halevi, L. Dobrzynski, and B. Djafari-Rouhani, Phys. Rev. Lett. **71**, 2022 (1993).
8. V. V. Tyutekin, Acoust. Phys. **49**, 721 (2003).
9. V. V. Tyutekin, Acoust. Phys. **52**, 733 (2006).
10. I. V. Andronov, Acoust. Phys. **56**, 259 (2010).
11. T. Gorishnyy, C. K. Ullal, M. Maldovan, G. Fytas, and E. L. Thomas, Phys. Rev. Lett. **94**, 115501 (2005).
12. J. J. Chen, K. W. Zhang, J. Gao, and J. C. Cheng, Phys. Rev. B **73**, 094307 (2006).
13. T. C. Wu, T. T. Wu, and J. C. Hsu, Phys. Rev. B **79**, 104306 (2009).
14. M. D. Guild, V. M. Garcíachocano, W. Kan, and J. Sanchezdehesa, J. Acoust. Soc. Am. **136**, 2076 (2014).
15. M. D. Guild, V. M. Garcíachocano, W. Kan, and J. Sánchezdehesa, J. Appl. Phys. **117**, 2539 (2015)
16. J. Mei, G. Ma, M. Yang, Z. Yang, W. Wen, and P. Sheng, Nat. Commun. **3**, 756 (2012).
17. W. Tempest, *Infrasound and Low Frequency Vibration* (Academic Press, London, 1976).
18. J. Mei, G. Ma, M. Yang, J. Yang, and P. Sheng, in *Acoustic Metamaterials and Phononic Crystals,* Ed. by P. A. Deymier (Springer, 2013).
19. A. Khelif, B. Aoubiza, S. Mohammadi, A. Adibi, and V. Laude, Phys. Rev. E **74**, 046610 (2006).
20. J. H. Wen, D. L. Yu, G. Wang, H. G. Zhao, Y. Z. Liu, and X. S. Wen, Chin. Phys. Lett. **24**, 1305 (2007).
21. J. Chen, Y. Xia, X. Han, and H. Zhang, Ultrasonics **52**, 920 (2012).
22. J. J. Chen, X. Han, and G. Y. Li, J. Appl. Phys. **113**, 184506 (2013).
23. T. T. Wu, Z. G. Huang, T. C. Tsai, and T. C. Wu, Appl. Phys. Lett. **93**, 111902 (2008).
24. Y. Pennec, B. Djafari-Rouhani, H. Larabi, J. O. Vasseur, and A. C. Hladky-Hennion, Phys. Rev. B **78**, 104105 (2008).
25. M. Oudich, Y. Li, B. M. Assouar, and Z. Hou, New J. Phys. **12**, 083049 (2010).
26. K. Yu, T. Chen, and X. Wang, Phys. B (Amsterdam, Neth.) **416**, 12 (2013).
27. H. Zhang, J. Chen, and X. Han, J. Appl. Phys. **112**, 054503 (2012).
28. J. Hsu, J. Phys. D: Appl. Phys. **44**, 055401 (2011).
29. Y. Xiao, J. Wen, and X. Wen, J. Phys. D: Appl. Phys. **45**, 195401 (2012).
30. M. B. Assouar and M. Oudich, Appl. Phys. Lett. **100**, 123506 (2012).
31. O. R. Bilal and M. I. Hussein, Appl. Phys. Lett. **103**, 111901 (2013).
32. P. Wang, T. Chen, K. Yu, and X. Wang, J. Appl. Phys. **113**, 053509 (2013).
33. H. J. Zhap, H. W. Guo, B. Y. Li, Z. Q. Deng, and R. Q. Liu, J. Appl. Phys. **118**, 044906 (2015).
34. M. B. Assouar, J. Sun, F. Lin, and J. Hsu, Ultrasonics **54**, 2159 (2014).
35. A. Bergamini, T. Delpero, L. D. Simoni, L. D. Lillo, M. Ruzzene, and P. Ermanni, Adv. Mater. **26**, 1343 (2014).
36. S. V. Kuznetsov, Acoust. Phys. **60**, 95 (2014).
37. P. Jiang, X. P. Wang, T. N. Chen, and J. Zhu, J. Appl. Phys. **117**, 154301(2015).
38. Y. G. Li, T. N. Chen, X. P. Wang, Y. H. Xi, and Q. X. Liang, Phys. Lett. A **379**, 412416 (2015).
39. S. Roundy, J. Intell. Mater. Syst. Struct. **16**, 809 (2005).
40. S. W. Zhang, J. H. Wu, and Z. P. Hu, J. Appl. Phys. **113**, 163511 (2013).
41. W. T. Thomson and M. D. Dahleh, *Theory of Vibration with Applications* (Tsinghua Univ. Press, Beijing, 2005).
42. S. B. Li, T. N. Chen, X. P. Wang, Y. G. Li, and W. H. Chen, Phys. Lett. A **380**, 2167 (2016).
43. S. B. Li, T. N. Chen, X. P. Wang, and Y. H. Xi, Mod. Phys. Lett. B **30**, 1650338 (2016).
44. S. B. Li, T. N. Chen, Y. H. Xi, and X. P. Wang, J. Xi'an Jiaotong Univ. **50**, 51 (2016).
45. Y. G. Li, L. Zhu, and T. N. Chen, Ultrasonics **73**, 34 (2017).
46. S. B. Li, Y. H. Xi, T. N. Chen, and X. P. Wang, Acoust. Phys. **63**, 508 (2017).
47. S. B. Li, Y. H. Dou, T. N. Chen, and Z. G. Wan, J. Xi'an Jiaotong Univ. **52**, 12 (2018).
48. J. P. Groby, J. Sanchezdehesa, and O. Umnova, Acta Acust. Acust. **104**, 5 (2018).
49. S. B. Li, Y. H. Dou, T. N. Chen, and Z. G. Wan, Mod. Phys. Lett. B **32**, 1850221 (2018).
50. B. Li, and K. T. Tan, Journal of Applied Physics, 120(7), 075103 (2016).
51. B. Li, S. Alamri and K.T. Tan, Scientific Reports 7(2017): 6226.
52. B. Li, K. T. Tan, and J. Christensen, Physical Review B, 95(14), 144305 (2017).
53. S. B. Li, Y. H. Dou, T. N. Chen, J. N. Xu, B. Li, and F. Zhang, Phys. Lett. A 383, 1371–1377 (2019).